Structure of As-Deposited and Heat-Treated Iron-Zinc Coatings from Chloride Bath*

C. A. Drewien
Sandia National Laboratories
Albuquerque, NM 87185

J. I. Goldstein and **A. R. Marder**
Lehigh University
Bethlehem, PA 18015

ABSTRACT

The iron content, phase constitution, and microstructure of electrodeposited iron-zinc alloy (EZA) coatings, deposited from chloride baths, is described for as-deposited and heat-treated conditions of coatings containing bulk iron contents of 6, 8, 10, and 13 w/o. The observed influence of current density upon iron content, which in turn influences the phase constitution and microstructure of the coatings, is reported. The microstructure, which is composed of non-equilibrium phases that have nanometer grain sizes, is illustrated and described with respect to iron content, crystallography, and morphology. As-deposited η phase coatings undergo transformations through a sequence of metastable phases when heated. The sequence of phase transformations varies with iron content, but the mechanisms of phase transformation from the as-deposited eta phase to the metastable G phase was found to be similar in 6, 8, and 10 w/o Fe coatings. Microstructural, compositional, and crystallographic changes associated with this phase transformation are discussed.

INTRODUCTION

Electrodeposited iron-zinc alloy (EZA) coatings are applied to steel sheet for corrosion protection of the underlying steel by both a barrier and a galvanic protection mechanism. These coatings mimic galvannealed coatings in that the presence of iron leads to improved weldability and paint adhesion of EZA coatings over pure zinc coatings (Adaniya et al., 1985), but the electrodeposited coating generally has greater ductility than its hot-dipped counter-part (Ike, 1984). EZA coatings therefore have found a niche in the automotive industry for the protection of steel sheet from corrosive attack by aggressive atmospheric and saline environments.

EZA coatings are commercially manufactured by co-depositing iron and zinc from a sulfate or chloride based electrodeposition bath. The co-deposition of two metals can lead to supersaturated solid solutions and non-equilibrium phases in the electrodeposited material. In fact, the supersaturation of zinc with iron to around 8 w/o and the presence of a non-equilibrium gamma phase have been reported by several investigators (Adaniya et al., 1985; Hara et al., 1983) who studied the structure and composition of EZA coatings produced from sulfate based baths. The microstructure of these coatings consisted of nanometer sized grains, and transformation of the original phases towards equilibrium phases in the iron-zinc binary system occurred with heat treatment to 300 °C (Gu, 1989). In this paper, the composition, phase constitution, and microstructure of as-deposited and heat-treated EZA coatings produced from chloride baths are presented.

---

* This work was funded by Rouge Steel, Kobe Steel, Lepel Corp., and ILZRO and supported in part by Sandia National Laboratories, which is operated for the U. S. Department of Energy under contract number DE-AC04-76DP00789.

DISCLAIMER

DISCLAIMER

Portions of this document may be illegible in electronic image products. Images are produced from the best available original document.

PROCEDURE

EZA coatings were deposited using U. S. Steel's rapid flow, circulating electrodeposition cell and their patented electrolyte (Johnson and Pfister, 1985), which contains ferrous and zinc chloride, chelating agents, and grain-refining agents held at 40 °C. In this set-up, a zinc anode lies parallel the steel sheet to be coated, and the steel sheet itself acts as the cathode. The flow rate of the electrolyte through the plating section was maintained at 80 m/min, as measured using a rotometer. Current density and time were varied in order to obtain coatings of 7 μm thickness.

The bulk iron content of the coatings was measured using standard titration techniques. The coatings on the steel substrate were dissolved in 10% sulfuric acid until hydrogen evolution ceased, then the solution was titrated with a standard 0.02 N potassium permanganate solution until the end-point was obtained.

Phase identification was determined from x-ray diffraction analysis, performed using a Philips XRG3100 x-ray generator with an APD 3720 automated diffractometer system operated at 45 kV and 30 mA. Copper Kα radiation, filtered with a nickel filter, was used to scan the samples from 2θ values of 25 to 90 degrees at a scan rate of 1 degree/min. A quartz standard was used to check to alignment accuracy of the diffractometer. Quantitative x-ray analysis required the integrated peak intensity of standards and samples. Standards of the various zinc-rich intermetallics in the iron-zinc binary system were prepared using pure (>99.99%) zinc and iron powder, mixing, and homogenizing at 600 °C in an evacuated quartz tube. X-ray diffraction patterns of the standards and samples were individually determined under the conditions described above, and then background subtraction and Kβ removal was performed using a computerized profile fitting routine so that the area under the peaks could be accurately integrated. The peaks were designated to a phase or phases, and the integrated intensities of a given phase I_a were divided by the integrated intensities of the pure (standard) phase I_a^o. The ratio was divided by the total number of peaks (N) contributing to phase A:

$$L_a = \left(\frac{1}{N_a}\right)\sum_{1}^{N_a}\left(\frac{I_a}{I_a^o}\right)$$

This value was divided by the corresponding value for the B phase to obtain the average intensity ratio L_{ab}, which is equal to the volume fraction ratio V_a/V_a:

$$L_{ab} = \frac{\left(\frac{1}{N_a}\right)\sum_{1}^{N_a}\left(\frac{I_a}{I_a^o}\right)}{\left(\frac{1}{N_b}\right)\sum_{1}^{N_b}\left(\frac{I_b}{I_b^o}\right)} = \frac{\mu_a}{\mu_b}\frac{V_a}{V_b}$$

The relationship that $V_a+V_b=1$ allowed for calculation of the volume fractions of the phases in the coatings, provided the linear absorption coefficients (μ) of the phases were known. The linear absorption coefficients used for η and G phases were 424 and 917, respectively.

Microstructural examination was performed using a JEOL 6300 FEG-SEM operated at an accelerating voltage of 1 or 10 kV or using a Philips 430 TEM operated at an accelerating voltage of 250 kV. Samples for TEM observation were prepared by electropolishing the coating, which was removed from the substrate, with a room-temperature chromic-acetic acid solution (Livak and Thomas, 1974). A Gatan single tilt

heating stage was used for in-situ heating studies in the TEM. Analytical electron microscopy (AEM) analysis was performed using a Philips 400 EM and a Tracor-Northern 2000 EDS detector. The characteristic x-ray spectra were obtained in STEM mode using a focused electron beam probe of 20 nm at an operating voltage of 120 kV. To find the concentration (C) of iron and zinc in the microstructural constituents, the measured intensities (I) were used in the Cliff-Lorimer thin film equation (Cliff and Lorimer, 1975):

$$\frac{C_A}{C_B} = k_{AB}\frac{I_A}{I_B}$$

where the k_{ZnFe} value was determined to be 1.25±0.15.

Heat treatment of the coated steel sheet was performed using a Gleeble thermomechanical testing unit at heating rates of 100 °C/s. Heat treatment of the coating removed from the substrate was performed in a Mettler differential scanning calorimeter (DSC) model 30 employing heating rates from 5 to 90°C/min.

AS-DEPOSITED COATINGS

The bulk iron content of the as-deposited coatings was dependent upon the current density used during electrodeposition. An increase in iron content occurred with an increase in the current density through the cell as shown in Table I. Despite the variation in iron content, the main phase in the coatings was eta (η) phase, or hexagonal close-packed zinc supersaturated with iron. The interplanar spacings of the eta phase varied with iron content to 8-9 w/o and then became constant, indicating that η phase contained 8 w/o Fe as compared to the equilibrium zinc-iron solid solution that contains about 0.23 w/o Fe. AEM analysis revealed that η phase contained 8 w/o±14%. Above a bulk iron content of 8 w/o minor amounts of a second phase were detected from x-ray diffraction analysis. This phase was body-centered cubic with a lattice parameter of 8.99 Å±1.1%, which is equal to the lattice parameter

TABLE I.--Current density, iron content, and phase constitution of as-deposited EZA coatings

Current density (A/m^2)	Iron Content (w/o)	% η phase (v/o)	% G phase (v/o)
8,450	6.1±0.3	100	
9,500	8.3±0.2	100	
10,550	10.2±0.25	99+	trace
12,600	12.9±0.15	99+	trace

of gamma (Γ) phase in the equilibrium iron-zinc binary system. Analysis of the gamma-like phase in the AEM yielded a iron content of 12 w/o ±14.2%, or a value lower than the minimum iron content contained by the equilibrium gamma phase (22 w/o at 300 °C). As such, the as-deposited EZA coatings from chloride baths exhibited an extended region of supersaturation for the solid solution of η and a non-equilibrium gamma-like phase, which will be referred to as G phase.

The appearance of the surface microstructure varied with bulk iron content in the coating, but some similarity in features was established. Crystallites of approximately 300-600 nm width containing growth ledges that were typically 30-50 nm in width were present on the surface of all coatings. An example of the surface morphology of the coatings is provided by the SEM micrograph of a coating containing 8 w/o bulk iron

shown in Figure 1. It was noted that coatings containing lower iron content exhibited greater porosity between adjacent crystallites than coatings with higher iron contents. The crystallites exhibited preferred orientation of the {11.0} planes. This preferred orientation, established by comparison of randomly-oriented zinc powder with the eta phase in the coatings (see Table II), is common in electrodeposited materials containing a hexagonal close-packed structure (Pangarov, 1964).

TABLE II.--Interplanar Spacings and Relative Peak Intensities for zinc and EZA as-deposited coatings containing bulk iron contents of 6, 8, 10, and 13 w/o

Plane	Zn d (Å)	Intensity of Zn peaks	6 w/o Fe d (Å)	Intensity of 6 w/o Fe η peaks	8 w/o Fe d (Å)	10 w/o Fe d (Å)	13 w/o Fe d (Å)
10.0	2.308	40	2.342	20	2.359	2.359	2.359
10.1	2.091	100	2.088	25	2.082	2.082	2.083
10.2	1.687	28	1.659	1	1.617	1.617	1.612
10.3	1.342	25	1.344	75			1.308
11.0	1.332	21	1.353	100	1.362	1.362	1.360
11.2	1.173	23	1.168	20	1.169	1.169	1.169

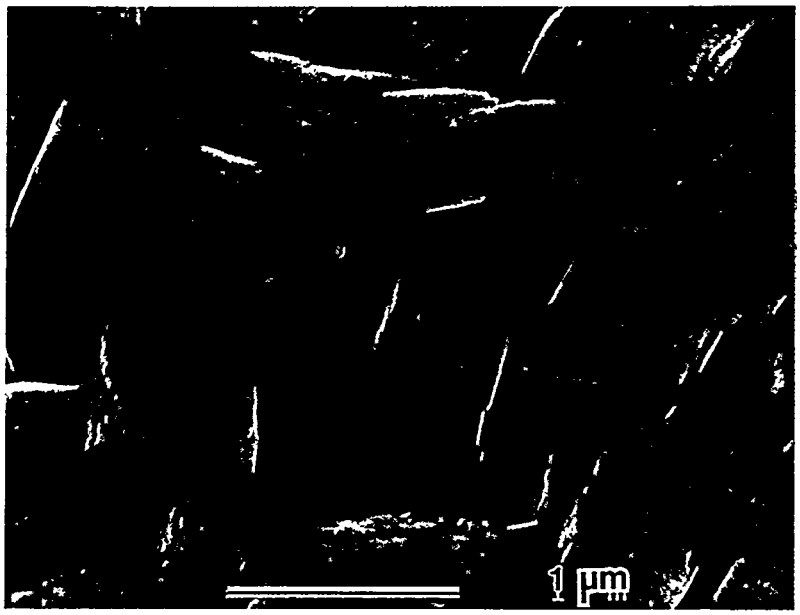

Figure 1.---SEM micrograph of the surface of as-deposited EZA coatings containing a bulk iron content of 8 w/o shows 500 nm wide crystallites and 30-50 nm wide ledges.

Subtle differences in the cross-sectional microstructure of the coatings were also detected based upon the iron content. The width of the crystallites (marked x) can be detected in the TEM micrograph of the 6 w/o Fe coating in Figure 2a, and within the crystallites the 30-50 nm wide linear ledge structure can also be detected (marked y). A final feature observed in the cross-sectional microstructure is the presence of fine streaks running parallel to the length of the ledges (see arrow); these streaks are barely observable in Figure 2b. It is believed that the streaks represent an amorphous phase, but the fine scale of the structure limited analysis as to the composition and no positive identification could be made. The differences detected in the cross-sectional microstructure due to iron content can be seen by comparing Figure 2a with Figure 2b.

The TEM micrograph in Figure 2b of the coating containing 13 w/o bulk iron differs from the 6 w/o Fe coatings, in that i.) the G phase is present as fine equiaxed grains (arrow labeled z) and ii.) the ledges are not as linear as in Figure 2a.

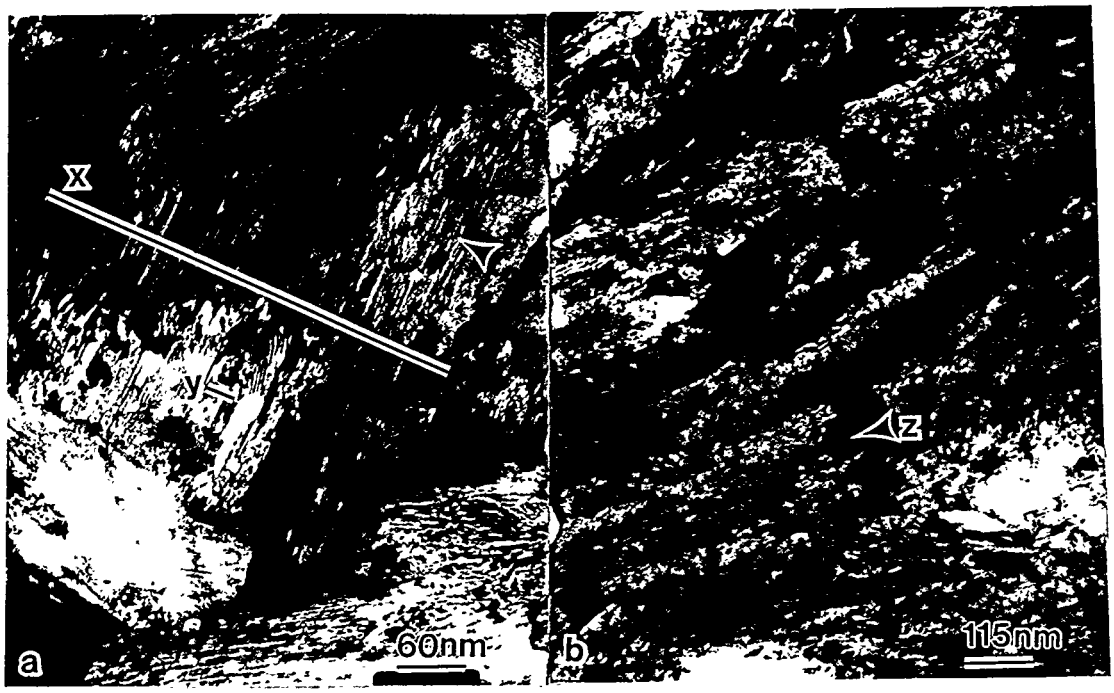

Figure 2.--TEM cross-sectional micrographs of EZA coatings containing a.) 6 and b.) 10 w/o bulk iron. x indicates crystallite width; y, ledge width; z, G phase grain.

The variation in appearance of the cross-sectional microstructure with iron content resulted from the nucleation of G phase, and some influence of recovery/polygonization may exist as the as-deposited coatings contain strain. The strain in the lattice due to the supersaturation of zinc with iron and the rapid rate of electrodeposition can be estimated from the width of the x-ray diffraction peaks. Peak widths for a 6 w/o Fe coating are provided in Table III. For the peak with an interplanar spacing (d) of 1.34 Å, whose width is 1.2°, a strain value of 0.04 can be calculated using the equation (Cullity, 1978):

$$B = 2\Delta\theta = 2\frac{\Delta d}{d}\tan\theta$$

where B is the breadth or width of the peak and θ is the Bragg angle for the reflection. To determine the strain value, some contribution of peak width due to small grain size effects was considered. This strain, which translates to a stress value of 10,000 kg/cm^2 for the **a** direction of pure zinc, and the temperature of the electrolyte during deposition (40°C) are sufficient to drive recovery in zinc. The recovery/polygonization effects are noticed in the microstructure by the change in width and length of the ledges, due to elimination of boundaries between adjacent ledges.

TABLE III.--X-ray diffraction peak width from η phase in as-deposited 6 w/o Fe EZA coatings	
Interplanar Spacing (Å)	Peak Width (°)
2.34	0.9
2.09	0.9
1.68	0.75
1.34, 1.33	1.85
1.17	0.75

HEAT-TREATED COATINGS

Heat treatment of the EZA coatings caused the coatings to transform from the as-deposited η phase into almost entirely G phase without undergoing any change in the bulk iron content of the coating. That is, 100 % G phase was detected in the coatings after the heat treatment through a cycle that was short enough to preclude long range diffusion of iron and zinc between the coating and the substrate. The iron content after heat treatment was the same value as measured before heat treatment. As mentioned, the G phase is crystallographically similar to the Γ phase, but the iron content of the G phase may be as low as 8 or 9 w/o. The interplanar spacings, relative peak intensities, and lattice parameters determined from x-ray diffraction data for the equilibrium Γ phase and the G phase are provided in Table IV. The high intensity of the {222} planes for the G phase in the EZA coatings suggested that these were preferentially oriented in the coatings. The orientation relationship (11.0)//(222) and [00.1]//[101] could exist between the parent η phase and product G phase.

The transformation temperature decreased with an increase in as-deposited bulk iron content, and the transformation kinetics increased with an increase in as-deposited bulk iron content indicating that the iron content greatly affected the transformation. The transformation itself was diffusion driven as evident from the time-temperature dependence obtained from the DSC and kinetics data. The peak temperatures obtained during heating the EZA coatings in the DSC at heating rates of 5 to 99°C/min increased with heating rate, as shown in Table V. In accordance with time and temperatures dependence, the temperature at which the maximum amount of material transformed increased with increased heating rate, because the shorter heating cycle required higher temperatures in order to transform the same volume of material. A time-temperature-transformation curve from isothermal heat treatment of EZA coatings using the Gleeble thermomechanical testing unit is shown in Figure 3. The samples were heated at 100 °C/s to peak temperatures indicated by the abscissa, held at temperature for the time indicated, and then water quenched to room temperature. The numbers in the phase fields containing η indicate the volume fraction of η determined by quantitative x-ray diffraction analysis. Again, diffusional behavior is indicated.

Activation energies for the η to G phase transformation were determined from the non-isothermal DSC data and the isothermal data using the Lee-Kim kinetics models (Lee and Kim, 1990a&b). The value from the isothermal data, given in Table VI, showed that a higher activation energy was required for transformation of the higher iron content coatings. However, once the activation energy was supplied, the transformation kinetics were more rapid for the higher iron content coatings than the lower iron content coatings. The increase in activation energy with iron content may be due to the values from the

TABLE IV.--Interplanar spacings, relative peak intensities, and lattice parameters for Γ phase (25 w/o Fe) and G phase (13 w/o Fe)				
Plane	Γ phase		G Phase	
	d (Å)	Intensity	d (Å)	Intensity
310	2.848	1		
222	2.599	5	2.590	100
321	2.405	5		
330,441	2.113	100	2.120	30
332	1.915	8	1.913	2
422	1.832	5	1.842	2
431,510	1.760	3	1.760	
530,433	1.546	1		
600,442	1.502	5	1.501	5
611,532	1.453	2		
622	1.349	1		
631	1.319	2		
444	1.291	5	1.293	25
710,550	1.267	6		
721,633	1.225	15	1.229	10
Lattice Parameters (Å)	8.98±1.8%		8.99±1.1%	

non-isothermal analysis are less accurate due to the small exothermic peak from which the data were extracted (see Figure 4); however, the confirmation of an activation energy value in the vicinity of 130 kJ/mole was realized. It should be emphasized that when more than one process is occurring simultaneously--i.e., recovery/polygonization and nucleation and growth of G phase--the significance of an activation energy may not be meaningless.

TABLE V.--Peak Temperature of Transformation from η to G Phase during non-isothermal heating at given heating rate				
Heating Rate (°C/min)	6 w/o Fe	8 w/o Fe	10 w/o Fe	13 w/o Fe
10	143	140	137.5	138.5
20	145		144.5	142
40			150	151
50	150	147	152	151.5
80	155	152		160
80	157	155	158	165

After the formation of G phase, continued heating to temperatures above 250 °C led to the further transformation of the G phase to the ζ' phase. The ζ' phase has been observed by Onishi et al. (1974) during heat treatment of electrodeposited zinc on steel. This phase contains an excess of iron compared to the equilibrium ζ phase in the binary iron-zinc system. Finally, the ζ' phase transforms near 300 °C to the δ phase if the bulk iron content of the as-deposited coatings was 6, 8, or 10 w/o or to the Γ_1 phase for the 13

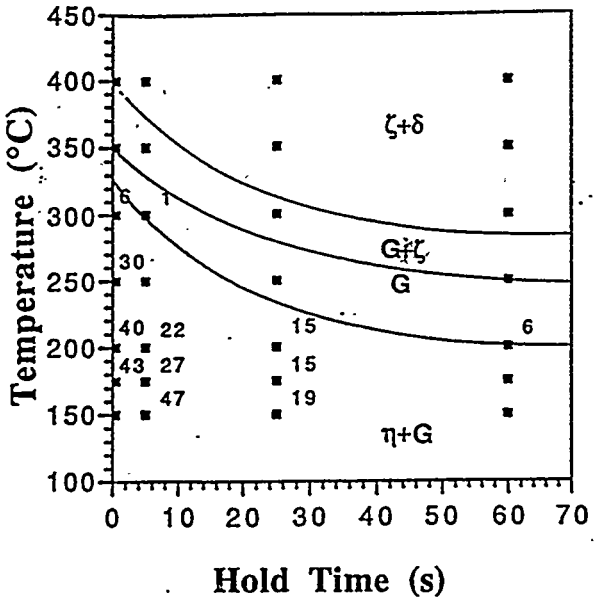

Figure 3.--Isothermal heat treatment data shown as a time-temperature-transformation diagram for the transformation of η to G in 10 w/o Fe coatings.

TABLE VI.--Activation energies for the η to G phase transformation in EZA coatings		
Iron content (w/o)	Activation Energy (kJ/mole) Isothermal Data	Activation Energy (kJ/mole) Non-isothermal Data
6	60	
8	77	132
10	106	125
13	129	129

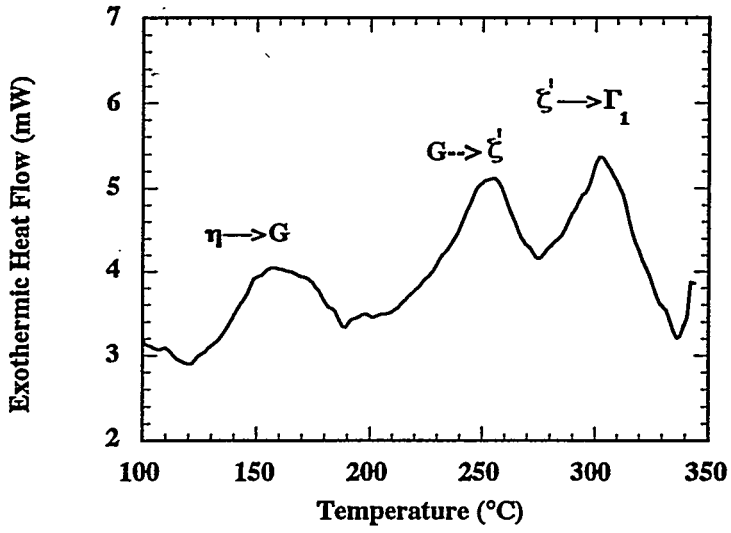

Figure 4.--DSC profile for 13 w/o Fe as-deposited coating heated at 99 °C/min contains three exothermic reactions.

w/o Fe coatings. A DSC profile showing the exothermic peaks of transformation is shown in Figure 4 for a coating initially containing 13 w/o bulk iron.

The TEM micrographs of in-situ heat treated coatings showed the sequence of the transformation from η to G phase occurred by the recovery/polygonization of the η phase ledges into shorter, wider segments followed by the nucleation and growth of the G phase into 30-50 nm equiaxed grains. The sequence is shown in Figure 5 for a 6 w/o Fe coatings where the arrow indicates a ledge in the a.) as-deposited structure,b.) is the microstructure after heat treating in-situ to 115 °C, c.) to 170 °C, and d.) to 215 °C.

DISCUSSION AND CONCLUSIONS

The as-deposited and heat-treated EZA coatings produced from a chloride-based electrodeposition bath were characterized for iron content, phase constitution, and microstructure. The coatings containing up to 13 w/o bulk Fe were comprised of η phase, a supersaturated solid solution of iron in hexagonal close-packed zinc. The eta phase was capable of dissolving up to 8-9 w/o Fe before the presence of a non-equilibrium gamma-like phase formed. The gamma-like phase, referred to as G phase, was body centered-cubic in structure and had the same lattice parameter as the equilibrium Γ phase in the binary iron-zinc system. The microstructure of the as-deposited coatings were comprised of 30-50 nm growth ledges and 300-600 nm crystallites, that exhibited preferred orientation of the {11.0} planes parallel to the plane of the substrate.

With heat treatment, the η phase transformed to G phase via a recovery/polygonization mechanism followed by nucleation of G phase. The transformation involved diffusion within the coating--that is, short range diffusion; no long range diffusion of zinc and iron between the coating and substrate occurred. The minimum iron content in G phase was about 8 w/o. With continued heating, the coatings continued to transform. In the case of 6, 8, and 10 w/o Fe the G phase transforms to ζ' then δ, while the 13 w/o Fe transforms from G to ζ' to Γ_1.

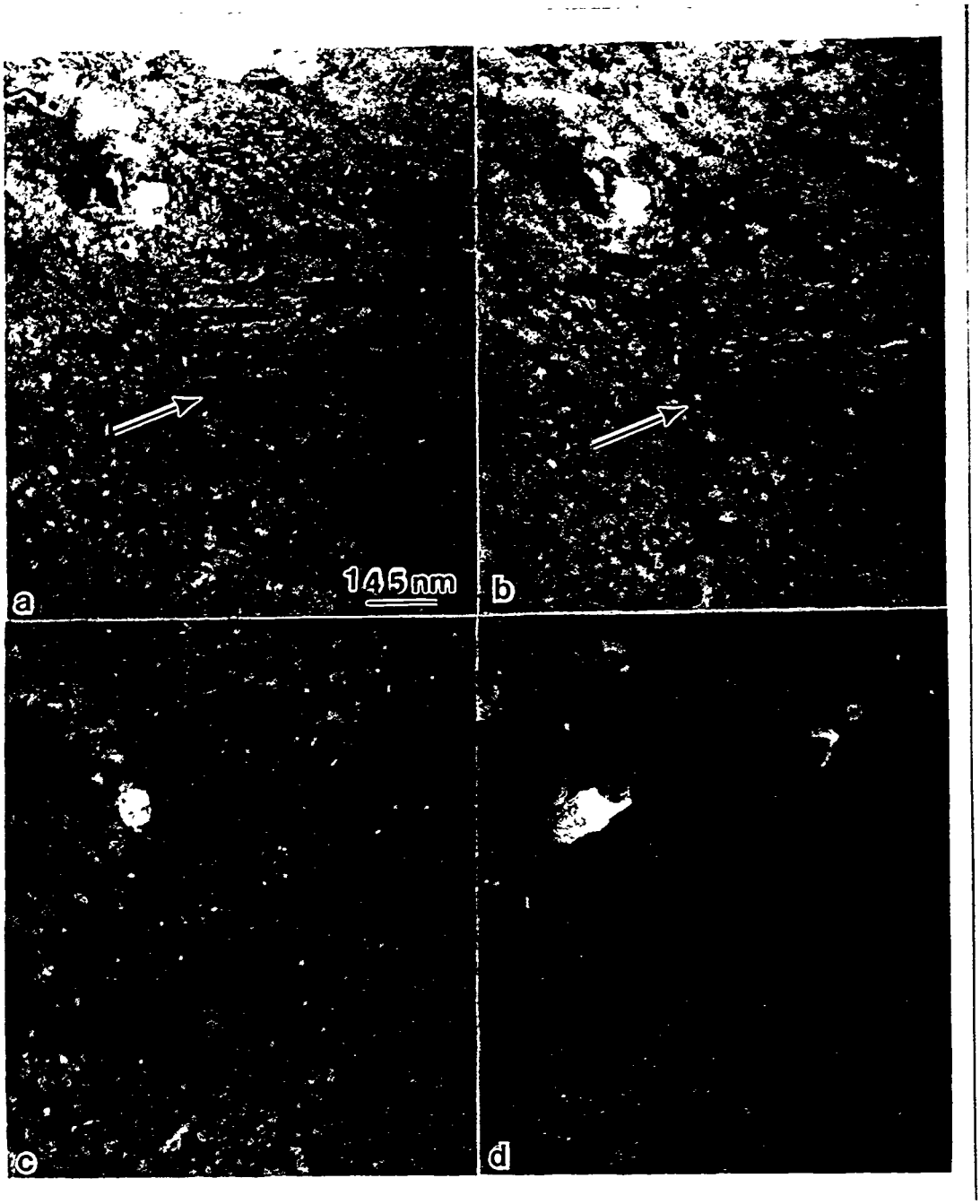

Figure 5.--In-situ heat treatment of a.) as-deposited 6 w/o Fe coating shows b.) recovery/polygonization of η phase leads to shorter, wider segments than the original ledges followed by c. and d.) nucleation and growth of G phase.

ACKNOWLEDGMENTS

The authors thank i.) J. Sheehan, C. J. Wu, J. Manack, and L. Pfister of U. S. Steel Corp. for their assistance in providing the samples used in this study, ii.) Rouge Steel, Kobe Steel, Lepel Corp. and International Lead and Zinc Research Organization for providing the funding for this study, and iii.) D. Ackland, A. O. Benscoter, and L. Barrett for their technical support.

REFERENCES

1. Adaniya, T., Hara, Y., Sagiyama, M., Honma, T., and Watanabe, T.: *Plating and Surface Finishing*, (1985) p. 52
2. Ike, H.: in Advanced Technology of Plasticity 1984, vol. 1 (1984) Proceedings of the First International Conference on Technology o Plasticity, Tokyo p. 180
3. Hara, T., Adaniya, T., Sagiyama, M., Honma, T., Tonouchi, A., Watanabe, T. and Ohmura, M.: *Trans. ISIJ*, **23** (1983) p. 954
4. Gu, M.: The Transformation from Non-Equilibrium to Equilibrium of Electrodeposited Zinc-Iron Alloy Coatings, Ph.D. dissertation, Lehigh University, Bethlehem, PA (1989)
5. Johnson, W. R. and Pfister, L. E.: U. S. Patent 4,540,472, *Official Gazette* (1985) p. 768
6. Livak, R. J. and Thomas, G.: *Acta Met..*, **22** (1974) p. 589
7. Cliff, G. and Lorimer, G. W.: *J. Microscopy*, **103** (1975) p. 203
8. Pangarov, N., A.: *Electrochima Acta*, **9** (1964) p. 721
9. Cullity, B. D.: Elements of X-ray Diffraction, 2nd edition, Addison-Wesley Publ. Co. Reading, MA (1978)
10. Lee, E. S. and Kim, Y. G.: *Acta Metall. Mater.*, **38**, (1990a) p. 1669
11. Lee, E. S. and Kim, Y. G.: *Acta Metall. Mater.*, **38** (1990b) p. 1677
12. Onishi, M., Wakamatsu, Y., and Miura, H.: *Trans. JIM*, **15** (1974) p. 331